J. Phys. B: At. Mol. Opt. Phys. **41** (2008) 235203 (12pp) doi:10.1088/0953-4075/41/23/235203

R-matrix inner-shell electron-impact excitation of Fe^{15+} including Auger-plus-radiation damping

G Y Liang, A D Whiteford and N R Badnell

Department of Physics, University of Strathclyde, Glasgow G4 0NG, UK

E-mail: guiyun.liang@strath.ac.uk

Received 11 September 2008, in final form 28 October 2008
Published 24 November 2008
Online at stacks.iop.org/JPhysB/41/235203

Abstract

We present results for the inner-shell electron-impact excitation of Fe^{15+} using the intermediate-coupling frame transformation *R*-matrix approach in which Auger-plus-radiation damping has been included. The target and close-coupling expansions are both taken to be the 134 levels belonging to the configurations $2s^22p^63l$, $2s^22p^53s3l$, $2s^22p^53p^2$ and $2s^22p^53p3d$. The comparison of Maxwell-averaged effective collision strengths with and without damping shows that the damping reduction is about 30–40% for many transitions at low temperatures, but up to 80% for a few transitions. As a consequence, the results of previous Dirac *R*-matrix calculations (Aggarwal and Keenan 2008 *J. Phys. B: At. Mol. Opt. Phys.* **41** 015701) overestimate the effective collision strengths due to their omission of Auger-plus-radiation damping.

(Some figures in this article are in colour only in the electronic version)

1. Introduction

Radiation from Fe^{15+} occupies a considerable fraction of the EUV and x-ray radiation spectrum of (the astrophysically abundant element) iron. Its temperature of peak fractional abundance is at $\approx 2.5 \times 10^6$ K in collision-dominated plasmas (Bryans *et al* 2006) and a few times 10^4 K in photoionized plasmas (Kallman and Bautista 2001). Observations of inner-shell excitation lines such as $2p^63s$–$2p^53l3l'$ in the solar corona have led to extensive investigations of inner-shell excitation data for this ion (see, e.g., Dere *et al* 2001).

Earlier calculations adopted the distorted-wave (DW) approximation. For example, Cornille *et al* (1994) reported excitation data amongst the lowest 44 levels belonging to the $2p^63s$ and $2p^53s3l$ (l = s, p and d) configurations. This data was adopted by Phillips *et al* (1997) to analyse the contribution of satellite lines to line-ratios, arising from inner-shell excitations, which are useful in solar diagnostic applications. Resonant excitation plays an important role in electron–ion collision processes, enhancing the effective collision strength (Υ), especially for forbidden transition lines. These lines are usually density and temperature sensitive and so have potential diagnostic applications. Bautista (2000) performed a standard *R*-matrix (Berrington *et al* 1995) calculation for inner-shell excitation which included the 134-levels belonging to the $2s^22p^63l$, $2s^22p^53s3l$, $2s^22p^53p^2$ and $2s^22p^53p3d$ (l = s, p and d) configurations (the same configurations considered in the present work). The enhancement of Maxwell-averaged effective collision strengths (Υ) by resonances in the ordinary collision strengths (Ω) was found to be up to three orders of magnitude at low temperatures, for some transitions. In Bautista's calculation, relativistic effects were included by using term-coupling coefficients (TCC) via the JAJOM code[1]. This changed the background collision strengths by up to an order of magnitude when compared to the results of his *LS*-coupling calculations, in which the algebraic splitting of scattering matrices was used to obtain the fine-structure data. Recently, Aggarwal and Keenan (2008) calculated inner-shell excitation data using the same 134-level target configurations with the fully-relativistic Dirac atomic *R*-matrix code (DARC) of Norrington and Grant (1987). Detailed comparisons with the excitation data of Bautista (2000) were made, and they pointed out deficiencies in the data of Bautista due to the methodology used by JAJOM.

[1] The TCCs were obtained from the *R*-matrix RECUPD code.

 © 2008 IOP Publishing Ltd Printed in the UK

In a detailed study of Fe^{14+}, Berrington *et al* (2005) found that the Breit–Pauli *R*-matrix effective collision strengths agreed with the DARC calculations to within 6%. For complex species, the number of (closely spaced) levels that must be included in the close-coupling (CC) expansion is very large, which makes the calculation computationally demanding. An alternative approach to a full Breit–Pauli *R*-matrix calculation is to perform an *R*-matrix calculation in *LS*-coupling and then, on making use of multi-channel quantum defect theory (MQDT), transform the resulting 'unphysical' *K*- or *S*-matrices to intermediate coupling. This eliminates at root the deficiency of JAJOM, namely, only transforming the open–open part of the physical *K*-matrix, since all channels are treated as being 'open' in MQDT. This is the intermediate coupling frame transformation (ICFT) method. In studying of the ICFT *R*-matrix electron excitation of Fe^{14+} and Ni^{4+}, Griffin *et al* (1998) and Badnell and Griffin (1999) found that the ICFT results agreed closely with those determined from the full Breit–Pauli *R*-matrix calculation. Another advantage of the ICFT method is the saving of computational time, which makes meaningful iso-electronic sequence calculations a reality within the *R*-matrix framework (Witthoeft *et al* 2007).

Resonances superimposed upon the background cross section enhance the effective collision strengths for electron-impact excitation, especially at lower temperatures and/or for weaker transitions. However, some resonant states may decay by an Auger process or fluorescence radiation and so are lost in the transition under study. Such loss mechanisms can be represented by a complex optical potential. Robicheaux *et al* (1995) provided a detailed description of radiation damping via such a potential within the *R*-matrix method. Subsequently, Gorczyca *et al* (1995) showed the effect of radiation damping on the electron-impact cross section of Ti^{20+} while Gorczyca and Badnell (1996) demonstrated its even greater importance for photorecombination. Gorczyca and Robicheaux (1999) extended the optical potential approach so as to include Auger damping. Whiteford *et al* (2002) demonstrated the Auger damping effect on the effective collision strengths of inner-shell transitions in Li-like Ar^{15+} and Fe^{23+}, and showed significant reductions in effective collision strengths at low temperatures ($\sim$30% for the $1s^2 2s\ ^2S_{1/2} - 1s2s^2\ ^2S_{1/2}$ transition of Fe^{23+}). Correspondingly, this has an influence on the spectroscopic diagnostic and modelling of plasmas, especially photoionized plasmas which typically have a much lower electron temperature. Furthermore, Bautista *et al* (2004) demonstrated the smearing of the photoabsorption K-edge by such damping, primarily Auger, for Fe^{16+} through Fe^{22+}.

In the present work we study the inner-shell electron-impact excitation of Fe^{15+}, via the *R*-matrix ICFT approach, using the same CC and CI expansions as in the work of Aggarwal and Keenan (2008) but now include Auger-plus-radiation damping. This work is a part of on-going collaborative work—the UK atomic processes for astrophysical plasmas (APAP) network[2], a broadening of scope of the original UK RmaX network. In section 2 we present details of our structure calculation and make comparisons with other data available in the literature. Our calculations for the scattering problem are detailed in section 3. The results, and their comparison with those of others, are discussed in section 4. We conclude with section 5.

2. Structure

We included the following configurations: $2s^2 2p^6 3l$, $2s^2 2p^5 3s3l$, $2s^2 2p^5 3p^2$ and $2s^2 2p^5 3p3d$. The orbital basis functions (1s–3d) were obtained from AUTOSTRUCTURE (Badnell 1986) using the Thomas–Femi–Dirac–Amaldi model potential (Eissner *et al* 1974). The radial scaling parameters were obtained by a two-step procedure of energy minimization. In the first step, the average energy of all 59 terms was minimized by allowing all scaling parameters (one for each *nl* orbital) to change. We then fixed the resulting radial scaling parameter of the 1s orbital ($\lambda_{1s} = 1.419\,58$). Finally, we minimized the average energy sum of all 134 levels, obtained from an intermediate coupling calculation, so as to determine the remaining scaling parameters. The resultant values are $\lambda_{2s} = 1.303\,24$, $\lambda_{2p} = 1.140\,32$, $\lambda_{3s} = 1.236\,27$, $\lambda_{3p} = 1.135\,55$ and $\lambda_{3d} = 1.006\,15$. (The mass–velocity plus Darwin contribution from the 1s orbital is too large for the minimization procedure to converge if the 1s scaling parameter is varied in intermediate coupling—the energy functional has no minimum.)

We compare our energies with the values available from the NIST database v3.0 [3] and the GRASP calculation of Aggarwal and Keenan (2007) (hereafter referred to as AK07). Their (AK07) calculations of structure used the same configurations as herein. The subsequent electron collision scattering calculations of Aggarwal and Keenan (2008) (hereafter, AK08) also used a structure determined by AK07. Excellent agreement (within 0.1%) is obtained when compared with the results of the AK07 GRASP calculation that omitted Breit and QED effects. The AK07 data is systematically higher than our results by less than 0.1 Ryd for the doubly-excited levels. The agreement with the NIST data is to within 0.5%, except for the $2s^2 2p^5 3s3d\ ^2D_{5/2}$, $^2F_{7/2}$, $^2F_{5/2}$ and $^2P_{3/2}$ levels. The difference is within 0.2% for these levels. Note, although AK07 obtained better agreement with the NIST data when Breit and QED effects were included, they are not present within DARC (nor two-body fine-structure within Breit–Pauli *R*-matrix) and so such a structure cannot be used in a scattering calculation.

Due to the strong configuration interaction and level mixing, as illustrated in table 1 of AK07, level orderings for comparisons are not the same in different calculations. Here, we match the level assignment according to configuration, total angular momentum and then energy ordering. Fortunately, only a few level assignments are inconsistent in the two different calculations, which facilitates our later comparisons for radiative decay rates (*A*-coefficients) and collision strengths. However, for some levels, their different assignments result in large discrepancies (up to 0.84 Ryd) with the NIST values in the AK07 work, such as for levels 11 and 14. Similar disturbed level ordering appears for levels

[2] http://amdpp.phys.strath.ac.uk/UK_APAP

[3] http://physics.nist.gov/PhysRefData/ASD/levels_form.html

Table 1. Energy levels (Ryd), and differences, for the $2s^22p^63l$, $2s^22p^53s3l$ (l = s, p and d), $2s^22p^53p^2$ and $2s^22p^53p3d$ configurations of Fe^{15+}.

Index	Configuration	$^{2S+1}L_J$	NIST[a]	AS[b]	GRASP[c]	FAC[d]	AS–NIST	GRASP–NIST
1	$2s^22p^63s$	$^2S_{1/2}$	0.000 00	0.000 00	0.000 00	0.000 00	0.000 00	0.000 00
2	$2s^22p^63p$	$^2P_{1/2}$	2.525 98	2.559 04	2.566 18	2.547 49	0.033 06	0.040 20
3	$2s^22p^63p$	$^2P_{3/2}$	2.716 88	2.766 60	2.754 86	2.736 95	0.049 72	0.037 98
4	$2s^22p^63d$	$^2D_{3/2}$	6.155 62	6.176 19	6.195 91	6.169 30	0.020 57	0.040 29
5	$2s^22p^63d$	$^2D_{5/2}$	6.182 09	6.217 36	6.220 81	6.194 88	0.035 27	0.038 72
6	$2s^22p^53s^2$	$^2P_{3/2}$	52.607 45	52.348 42	52.317 94	52.413 68	−0.259 03	−0.289 51
7	$2s^22p^53s^2$	$^2P_{1/2}$	53.518 71	53.287 28	53.240 28	53.333 65	−0.231 43	−0.278 43
8	$2s^22p^53s3p$	$^4S_{3/2}$		54.117 60	54.083 74	54.176 77		
9	$2s^22p^53s3p$	$^4D_{5/2}$	54.511 99	54.365 41	54.329 40	54.426 27	−0.146 58	−0.182 59
10	$2s^22p^53s3p$	$^4D_{7/2}$		54.413 66	54.381 45	54.476 48		
11	$2s^22p^53s3p$	$^2P_{3/2}$		54.424 11	54.389 38	54.489 68		
12	$2s^22p^53s3p$	$^2P_{1/2}$	54.685 14	54.551 54	54.520 45	54.619 49	−0.133 60	−0.164 69
13	$2s^22p^53s3p$	$^4P_{5/2}$		54.653 36	54.624 89	54.725 04		
14	$2s^22p^53s3p$	$^2D_{3/2}$	54.794 42	54.656 85	54.628 69	54.730 60	−0.137 57	−0.165 73
15	$2s^22p^53s3p$	$^2S_{1/2}$	55.058 76	54.879 78	54.844 42	54.939 87	−0.178 98	−0.214 34
16	$2s^22p^53s3p$	$^4D_{1/2}$	55.359 47	55.264 94	55.213 06	55.308 85	−0.094 53	−0.146 41
17	$2s^22p^53s3p$	$^4D_{3/2}$	55.487 05	55.358 90	55.307 39	55.404 41	−0.128 15	−0.179 66
18	$2s^22p^53s3p$	$^4P_{1/2}$	55.487 05	55.378 35	55.336 84	55.428 04	−0.108 70	−0.150 21
19	$2s^22p^53s3p$	$^4P_{3/2}$	55.550 84	55.478 99	55.435 83	55.529 46	−0.071 85	−0.115 01
20	$2s^22p^53s3p$	$^2D_{5/2}$		55.479 04	55.444 67	55.530 84		
21	$2s^22p^53s3p$	$^2D_{5/2}$	55.678 42	55.548 16	55.504 69	55.600 98	−0.130 26	−0.173 73
22	$2s^22p^53s3p$	$^2P_{3/2}$	55.851 56	55.614 25	55.586 97	55.674 45	−0.237 31	−0.264 59
23	$2s^22p^53s3p$	$^2P_{1/2}$		56.298 95	56.256 43	56.343 56		
24	$2s^22p^53s3p$	$^2D_{3/2}$	56.653 47	56.456 16	56.409 48	56.490 89	−0.197 31	−0.243 99
25	$2s^22p^53s3p$	$^2S_{1/2}$	57.109 11	57.016 87	56.993 70	57.085 92	−0.092 24	−0.115 41
26	$2s^22p^53p^2$	$^4P_{3/2}$		57.104 17	57.067 04	57.156 30		
27	$2s^22p^53p^2$	$^2P_{1/2}$		57.104 68	57.064 88	57.159 17		
28	$2s^22p^53p^2$	$^4P_{5/2}$		57.173 52	57.139 44	57.227 99		
29	$2s^22p^53p^2$	$^2F_{7/2}$		57.192 33	57.148 06	57.244 27		
30	$2s^22p^53p^2$	$^2P_{3/2}$		57.265 44	57.227 68	57.320 10		
31	$2s^22p^53p^2$	$^2D_{5/2}$		57.389 43	57.351 18	57.447 27		
32	$2s^22p^53p^2$	$^2D_{3/2}$		57.425 87	57.391 27	57.486 31		
33	$2s^22p^53p^2$	$^4P_{1/2}$		57.440 09	57.405 47	57.495 46		
34	$2s^22p^53p^2$	$^4D_{7/2}$		57.453 69	57.421 05	57.512 16		
35	$2s^22p^53p^2$	$^4D_{5/2}$		57.469 57	57.437 29	57.530 05		
36	$2s^22p^53p^2$	$^4D_{1/2}$		57.931 00	57.874 58	57.965 58		
37	$2s^22p^53p^2$	$^4S_{3/2}$		57.962 40	57.917 73	58.011 94		
38	$2s^22p^53s3d$	$^4P_{1/2}$		58.031 32	57.938 88	58.029 76		
39	$2s^22p^53s3d$	$^4P_{3/2}$		58.100 48	58.005 38	58.096 16		
40	$2s^22p^53p^2$	$^2F_{5/2}$		58.182 27	58.127 51	58.184 95		
41	$2s^22p^53p^2$	$^4D_{3/2}$		58.196 72	58.095 55	58.207 98		
42	$2s^22p^53s3d$	$^4F_{9/2}$		58.197 37	58.141 56	58.219 59		
43	$2s^22p^53s3d$	$^4P_{5/2}$	58.257 30	58.219 84	58.117 94	58.230 81	−0.037 46	−0.139 36
44	$2s^22p^53s3d$	$^4F_{7/2}$		58.249 83	58.161 02	58.247 24		
45	$2s^22p^53p^2$	$^2S_{1/2}$		58.263 94	58.211 89	58.300 63		
46	$2s^22p^53s3d$	$^4F_{5/2}$	58.375 77	58.324 13	58.243 86	58.329 35	−0.051 64	−0.131 91
47	$2s^22p^53p^2$	$^2D_{3/2}$		58.398 17	58.367 42	58.427 91		
48	$2s^22p^53s3d$	$^2D_{3/2}$		58.427 14	58.343 52	58.453 25		
49	$2s^22p^53s3d$	$^4D_{7/2}$	58.521 57	58.474 11	58.395 64	58.477 94	−0.047 46	−0.125 93
50	$2s^22p^53p^2$	$^2D_{5/2}$		58.480 76	58.438 27	58.507 28		
51	$2s^22p^53p^2$	$^2P_{3/2}$	58.548 91	58.500 36	58.422 42	58.530 72	−0.048 55	−0.126 49
52	$2s^22p^53s3d$	$^2F_{5/2}$		58.503 83	58.454 93	58.538 80		
53	$2s^22p^53s3d$	$^2P_{1/2}$	58.530 68	58.546 73	58.480 29	58.565 73	0.016 05	−0.050 39
54	$2s^22p^53s3d$	$^2P_{3/2}$	58.64915	58.72397	58.662 34	58.743 15	0.074 82	0.013 19
55	$2s^22p^53s3d$	$^4D_{1/2}$		58.813 95	58.760 90	58.835 84		
56	$2s^22p^53s3d$	$^4D_{3/2}$	58.986 32	59.112 74	59.043 24	59.120 33	0.126 42	0.056 92
57	$2s^22p^53s3d$	$^4F_{3/2}$		59.224 37	59.140 77	59.206 37		
58	$2s^22p^53s3d$	$^2F_{7/2}$	58.731 16	59.224 99	59.134 97	59.227 47	0.493 83	0.403 81
59	$2s^22p^53s3d$	$^4D_{5/2}$	59.250 58	59.250 61	59.153 03	59.233 82	0.000 03	−0.097 55
60	$2s^22p^53s3d$	$^2D_{5/2}$	58.904 30	59.295 65	59.204 74	59.282 33	0.391 35	0.300 44
61	$2s^22p^53s3d$	$^2F_{7/2}$	59.387 27	59.351 48	59.251 37	59.332 62	−0.035 79	−0.135 90

Table 1. (Continued.)

Index	Configuration	$^{2S+1}L_J$	NIST	AS	GRASP	FAC	AS–NIST	GRASP–NIST
62	$2s^22p^53p^2$	$^2P_{1/2}$		59.416 94	59.345 93	59.415 07		
63	$2s^22p^53s3d$	$^2D_{5/2}$	59.378 16	59.421 56	59.340 82	59.428 44	0.043 40	−0.037 34
64	$2s^22p^53p^2$	$^2P_{1/2}$		59.522 44	59.479 71	59.557 88		
65	$2s^22p^53p^2$	$^2P_{3/2}$		59.595 73	59.552 98	59.631 94		
66	$2s^22p^53s3d$	$^2D_{3/2}$		59.730 85	59.688 22	59.749 83		
67	$2s^22p^53s3d$	$^2P_{1/2}$	59.906 70	59.958 97	59.951 60	60.011 29	0.052 27	0.044 90
68	$2s^22p^53p3d$	$^4D_{1/2}$		60.133 69	60.046 11	60.134 89		
69	$2s^22p^53p3d$	$^4D_{3/2}$		60.206 90	60.118 29	60.196 17		
70	$2s^22p^53s3d$	$^2F_{5/2}$	59.742 67	60.229 59	60.128 42	60.207 05	0.486 92	0.385 75
71	$2s^22p^53p3d$	$^4D_{5/2}$		60.321 95	60.232 38	60.320 59		
72	$2s^22p^53p3d$	$^4G_{7/2}$		60.437 67	60.352 33	60.438 39		
73	$2s^22p^53p3d$	$^4G_{9/2}$		60.462 85	60.373 02	60.462 92		
74	$2s^22p^53s3d$	$^2P_{3/2}$	60.098 06	60.465 53	60.402 30	60.471 52	0.367 47	0.304 24
75	$2s^22p^53p3d$	$^4D_{7/2}$		60.475 14	60.385 02	60.473 72		
76	$2s^22p^53p3d$	$^4G_{11/2}$		60.504 04	60.410 11	60.500 21		
77	$2s^22p^53p3d$	$^2D_{5/2}$		60.525 99	60.447 77	60.530 85		
78	$2s^22p^53p3d$	$^2P_{3/2}$		60.572 79	60.486 75	60.573 93		
79	$2s^22p^53p3d$	$^4F_{5/2}$		60.634 53	60.556 05	60.637 74		
80	$2s^22p^53p3d$	$^2F_{7/2}$		60.638 82	60.548 20	60.641 32		
81	$2s^22p^53p3d$	$^2P_{1/2}$		60.692 41	60.601 83	60.693 57		
82	$2s^22p^53p3d$	$^2G_{7/2}$		60.743 57	60.670 77	60.756 21		
83	$2s^22p^53p3d$	$^4P_{1/2}$		60.835 23	60.735 33	60.823 00		
84	$2s^22p^53p3d$	$^4F_{9/2}$		60.840 00	60.768 30	60.852 78		
85	$2s^22p^53p3d$	$^4P_{3/2}$		60.865 06	60.771 71	60.857 69		
86	$2s^22p^53p3d$	$^4S_{3/2}$		60.908 03	60.816 15	60.900 62		
87	$2s^22p^53p3d$	$^4D_{7/2}$		60.923 32	60.828 74	60.914 66		
88	$2s^22p^53p3d$	$^4F_{5/2}$		60.943 96	60.853 44	60.936 10		
89	$2s^22p^53p3d$	$^4P_{5/2}$		60.953 86	60.859 14	60.941 13		
90	$2s^22p^53p3d$	$^2D_{3/2}$		60.986 20	60.914 94	60.993 07		
91	$2s^22p^53p3d$	$^2P_{3/2}$		61.057 53	60.964 48	61.040 79		
92	$2s^22p^53p3d$	$^4F_{9/2}$		61.060 44	60.955 73	61.046 87		
93	$2s^22p^53p3d$	$^4D_{5/2}$		61.096 88	61.018 01	61.097 55		
94	$2s^22p^53p3d$	$^4F_{7/2}$		61.129 62	61.037 64	61.121 45		
95	$2s^22p^53p3d$	$^2F_{5/2}$		61.147 34	61.063 69	61.146 24		
96	$2s^22p^53p3d$	$^4D_{7/2}$		61.169 98	61.084 98	61.162 28		
97	$2s^22p^53p3d$	$^2P_{1/2}$		61.187 77	61.110 25	61.188 41		
98	$2s^22p^53p3d$	$^2D_{3/2}$		61.254 89	61.182 34	61.261 36		
99	$2s^22p^53p3d$	$^4D_{5/2}$		61.276 70	61.202 05	61.280 70		
100	$2s^22p^53p3d$	$^2D_{3/2}$		61.329 68	61.248 93	61.324 73		
101	$2s^22p^53p3d$	$^4G_{5/2}$		61.340 88	61.245 85	61.331 04		
102	$2s^22p^53p3d$	$^4D_{1/2}$		61.412 49	61.353 21	61.423 49		
103	$2s^22p^53p3d$	$^2F_{5/2}$		61.433 93	61.344 45	61.425 16		
104	$2s^22p^53p3d$	$^2S_{1/2}$		61.494 22	61.424 43	61.488 94		
105	$2s^22p^53p3d$	$^4F_{3/2}$		61.499 58	61.402 08	61.500 40		
106	$2s^22p^53p3d$	$^4F_{7/2}$		61.517 01	61.422 21	61.506 76		
107	$2s^22p^53p3d$	$^2F_{5/2}$		61.572 11	61.473 47	61.557 45		
108	$2s^22p^53p3d$	$^2F_{7/2}$		61.650 79	61.560 56	61.640 55		
109	$2s^22p^53p3d$	$^2G_{9/2}$		61.678 35	61.581 75	61.663 70		
110	$2s^22p^53p3d$	$^4D_{3/2}$		61.697 01	61.614 93	61.687 24		
111	$2s^22p^53p3d$	$^2G_{9/2}$		61.793 28	61.693 34	61.765 35		
112	$2s^22p^53p3d$	$^4F_{3/2}$		61.826 96	61.721 11	61.802 85		
113	$2s^22p^53p3d$	$^2D_{5/2}$		61.898 47	61.800 37	61.874 59		
114	$2s^22p^53p3d$	$^2D_{5/2}$		61.961 61	61.865 16	61.939 45		
115	$2s^22p^53p3d$	$^4P_{1/2}$		61.976 06	61.889 79	61.962 75		
116	$2s^22p^53p3d$	$^2F_{7/2}$		61.990 48	61.899 80	61.968 94		
117	$2s^22p^53p3d$	$^2P_{3/2}$		62.008 86	61.914 57	61.987 90		
118	$2s^22p^53p3d$	$^4P_{5/2}$		62.044 87	61.948 88	62.020 41		
119	$2s^22p^53p3d$	$^4D_{1/2}$		62.065 20	61.979 98	62.057 19		
120	$2s^22p^53p3d$	$^4D_{3/2}$		62.068 35	61.978 02	62.060 89		
121	$2s^22p^53p3d$	$^2F_{7/2}$		62.105 21	61.996 87	62.075 02		
122	$2s^22p^53p3d$	$^2D_{5/2}$		62.115 42	62.021 63	62.096 05		
123	$2s^22p^53p3d$	$^2D_{3/2}$		62.123 17	62.050 18	62.113 36		

Table 1. (Continued.)

Index	Configuration	$^{2S+1}L_J$	NIST	AS	GRASP	FAC	AS–NIST	GRASP–NIST
124	$2s^22p^53p3d$	$^2D_{3/2}$		62.294 18	62.276 80	62.322 94		
125	$2s^22p^53p3d$	$^2D_{5/2}$		62.338 71	62.283 42	62.342 67		
126	$2s^22p^53p3d$	$^2P_{1/2}$		62.369 79	62.318 59	62.379 20		
127	$2s^22p^53p3d$	$^2P_{3/2}$		62.540 02	62.504 35	62.557 42		
128	$2s^22p^53p3d$	$^2S_{1/2}$		62.713 07	62.700 84	62.748 91		
129	$2s^22p^53p3d$	$^2G_{7/2}$		62.834 19	62.723 76	62.792 11		
130	$2s^22p^53p3d$	$^2F_{5/2}$		62.893 39	62.833 99	62.882 08		
131	$2s^22p^53p3d$	$^4P_{3/2}$		62.941 92	62.862 70	62.922 42		
132	$2s^22p^53p3d$	$^2P_{1/2}$		63.108 50	63.036 38	63.089 32		
133	$2s^22p^53p3d$	$^2D_{3/2}$		63.279 28	63.210 48	63.295 28		
134	$2s^22p^53p3d$	$^2D_{5/2}$		63.358 11	63.273 58	63.368 69		

[a] http://physics.nist.gov/PhysRefData/ASD/levels_form.html
[b] AUTOSTRUCTURE (present work).
[c] Aggarwal and Keenan (2007).
[d] Present work.

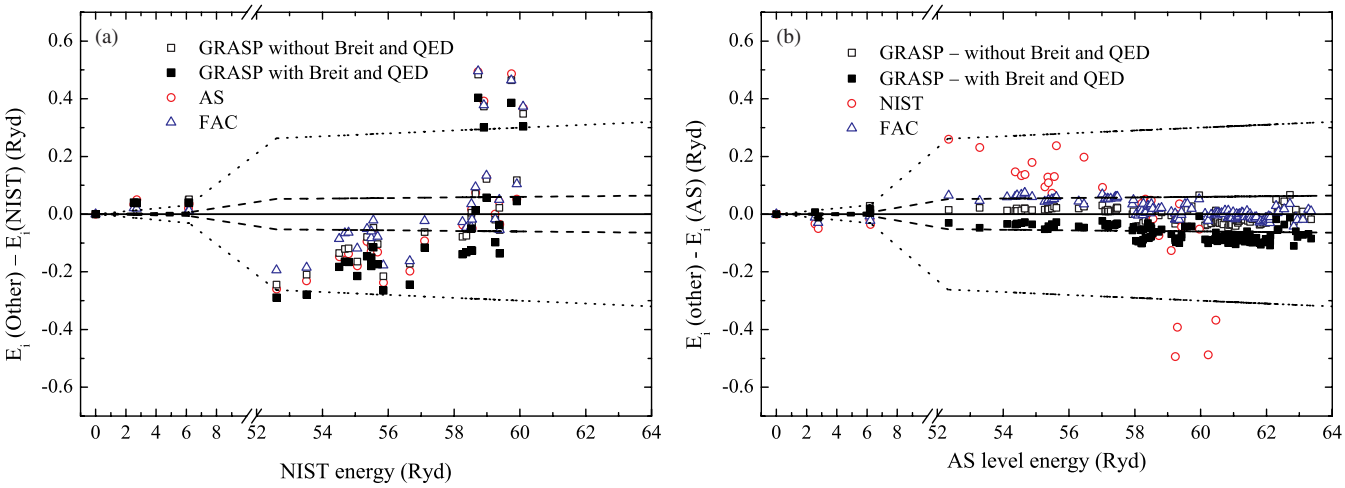

Figure 1. Comparisons of energy levels from the present AUTOSTRUCTURE (AS), GRASP (AK07) and FAC (present work) calculations. (a) Differences relative to the available experimental values (NIST database) versus the NIST data. Opened and filled square symbols correspond to the GRASP results, without and with the inclusion of Breit and QED effects, respectively (AK07); triangle symbols indicate the present FAC results; opened circles denote the present AS results. (b) The differences relative to the present AS results versus the present AS results. Symbols as before. The dashed and dotted lines correspond to agreement within 0.1% and 0.5%, respectively.

19/20, 26/27, 62/63 etc. Our new assignment eliminates the mis-order compared to the NIST values, as shown in table 1.

We also performed a structure calculation with the flexible atomic code (FAC) of Gu (2003), which shows slightly better agreement with our AUTOSTRUCTURE results than those from GRASP. Both are systematically higher than GRASP's, FAC more so. The results of the three different calculations are compiled in table 1, along with NIST data.

In the scatter plot of figure 2, we compare radiative decay rates ($A_{i,j}$ for the $i \leftarrow j$ transition) for all electric and magnetic multipoles from our AUTOSTRUCTURE calculation with the GRASP data from AK07 for decays to the lowest 5-lying levels. Electric dipole line strengths are also shown. Rates for some electric dipole transitions to the ground state are listed in table 2. For two-thirds of the transitions, the results of the two calculations agree to within 20%, and 95% of transitions agree to within a factor of 2. We also note that there are differences of more than a factor of 2, and up to an order of magnitude for few transitions, which may be due to the mismatch of the mapping of energy levels according to the parity, total angular momentum and energy order scheme in the two different calculations. Overall, the agreement is satisfactory.

3. Scattering

For the present case of Fe^{15+}, the resonance state configurations are of the form $[2s, 2p]^{q-1}[3s, 3p, 3d]^2 nl$ (here $q = 8, n \geqslant 3$), and they can decay via the following channels:

$$[2s, 2p]^{q-1}[3s, 3p, 3d]^2 nl \rightarrow [2s, 2p]^q[3s, 3p, 3d] + e^- \quad (1)$$

$$\rightarrow [2s, 2p]^q nl + e^- \quad (2)$$

$$\rightarrow [2s, 2p]^q[3s, 3p, 3d]^2 + h\nu \quad (3)$$

$$\rightarrow [2s, 2p]^q[3s, 3p, 3d]nl + h\nu. \quad (4)$$

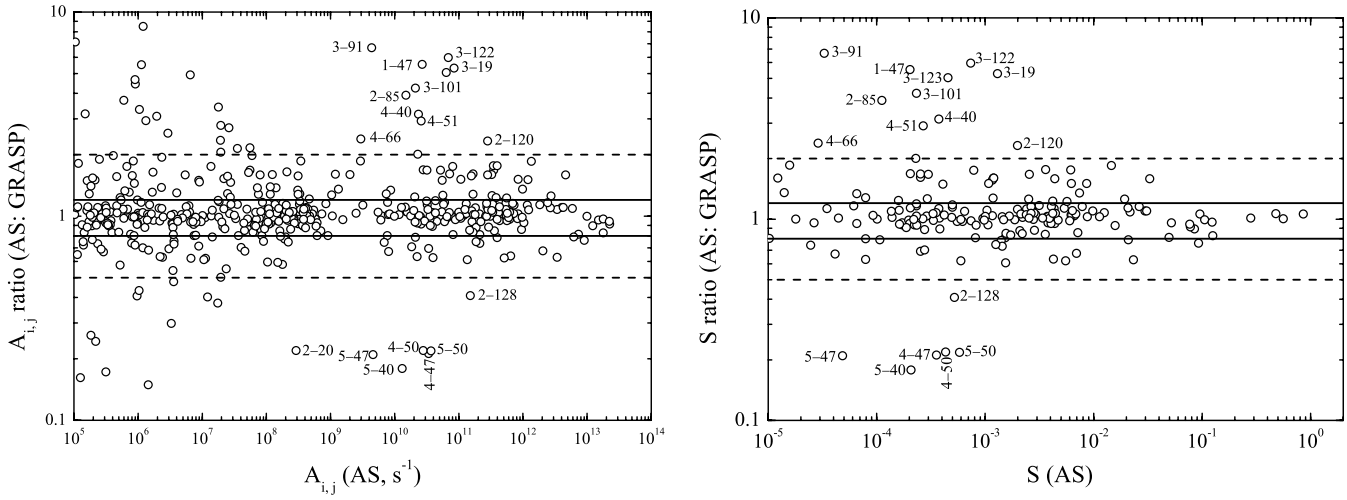

Figure 2. Comparison of radiative decay rates, $A_{i,j}$, (all multipoles) and electric dipole line strengths (S) from the present AUTOSTRUCTURE (AS) calculation and the GRASP calculation by AK07 for transitions to the lowest five levels. Solid and dashed lines correspond to agreement within 20% and a factor of 2, respectively. Transitions with differences of more than a factor of 2 are marked by the transition label. (In the case of the rates, labelling is restricted to strong rates: $\gtrsim 10^9\ \mathrm{s}^{-1}$.)

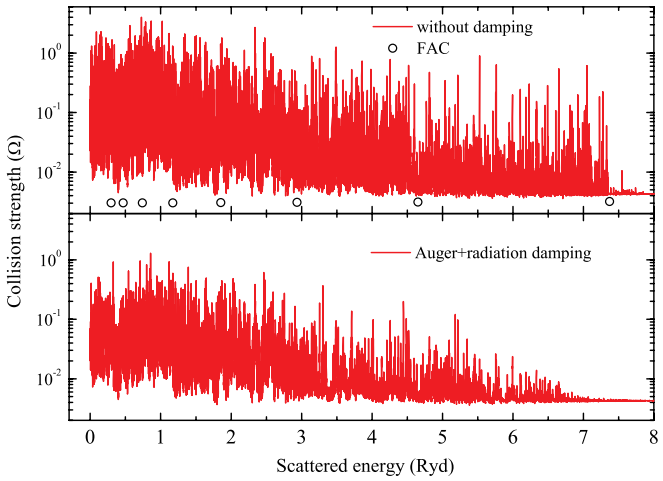

Figure 3. ICFT R-matrix excitation collision strengths for the $2s^2 2p^6 3s\ ^2S_{1/2}$–$2s^2 2p^5 3s^2\ ^2P_{3/2}$ transition, without damping (top) and Auger-plus-radiation damping (bottom). The circle symbols represent the results of our FAC DW calculation.

The participator LMn Auger pathway (1) scales as n^{-3} and is automatically described in the R-matrix method by the contribution to the close-coupling expansion from the right-hand side of (1). However, the spectator LMM Auger pathway (2) is independent of n and only low-n resonances ($n \leqslant 3$ here) can be included in the close-coupling expansion. But, the spectator Auger pathway dominates for $n > 3$. The last two channels, (3) and (4), represent radiation damping. These Auger and radiation damping processes reduce the resonant enhancement of the excitation collision strengths and can be expected to be especially important for inner-shell transitions due to the large energy jump.

For the Auger process, the participator Auger channel can be included explicitly within the R-matrix close-coupling expansion, whereas the spectator Auger decay cannot easily be included for the higher-n resonances as it requires the inclusion of target states with nl (with $n > 3$) orbitals. (So, only the Auger damping from $n = 3$ resonances has been included in the work of AK08.)

Table 2. Electric dipole radiative rates.

i	j	AS[a]	GRASP[b]	FAC[c]
1	2	6.071(09)[d]	6.283(09)	6.303(09)
1	3	7.542(09)	7.834(09)	7.884(09)
1	6	8.553(11)	8.202(11)	6.465(11)
1	7	8.317(11)	8.450(11)	6.666(11)
1	26	9.461(10)	9.327(10)	8.946(10)
1	27	3.088(11)	3.087(11)	2.991(11)
1	30	1.199(11)	1.187(11)	1.188(11)
1	33	8.400(10)	8.529(10)	8.788(10)
1	36	6.020(10)	5.136(10)	6.060(10)
1	37	2.067(10)	1.664(10)	2.180(10)
1	38	4.509(10)	4.774(10)	4.486(10)
1	39	9.727(10)	9.867(10)	9.301(10)
1	41	8.636(09)	6.427(09)	7.977(09)
1	47	2.700(10)	4.872(09)	5.000(10)
1	48	3.379(10)	4.862(10)	5.315(09)
1	51	1.473(10)	5.425(08)	1.757(08)
1	53	1.161(12)	1.025(12)	1.000(12)
1	54	4.042(12)	3.670(12)	3.545(12)
1	55	3.413(12)	3.161(12)	3.205(12)
1	56	1.197(12)	7.926(11)	9.465(11)
1	57	2.133(11)	2.632(11)	2.790(11)
1	62	3.950(11)	5.031(11)	4.780(11)
1	64	7.181(10)	4.447(10)	1.723(11)
1	65	2.730(12)	2.170(12)	3.221(12)
1	66	1.217(13)	1.359(13)	1.145(13)
1	67	2.254(13)	2.461(13)	2.260(13)
1	74	7.338(12)	9.012(12)	8.160(12)

[a] AUTOSTRUCTURE (present work).
[b] Aggarwal and Keenan (2007).
[c] Present work.
[d] (m) denotes $\times 10^m$.

We employ the R-matrix intermediate-coupling frame transformation (ICFT) method of Griffin *et al* (1998) allowing for both Auger-plus-radiation damping via the complex optical potential, as described above. We used 25 continuum basis per orbital angular momentum. Contributions from partial waves

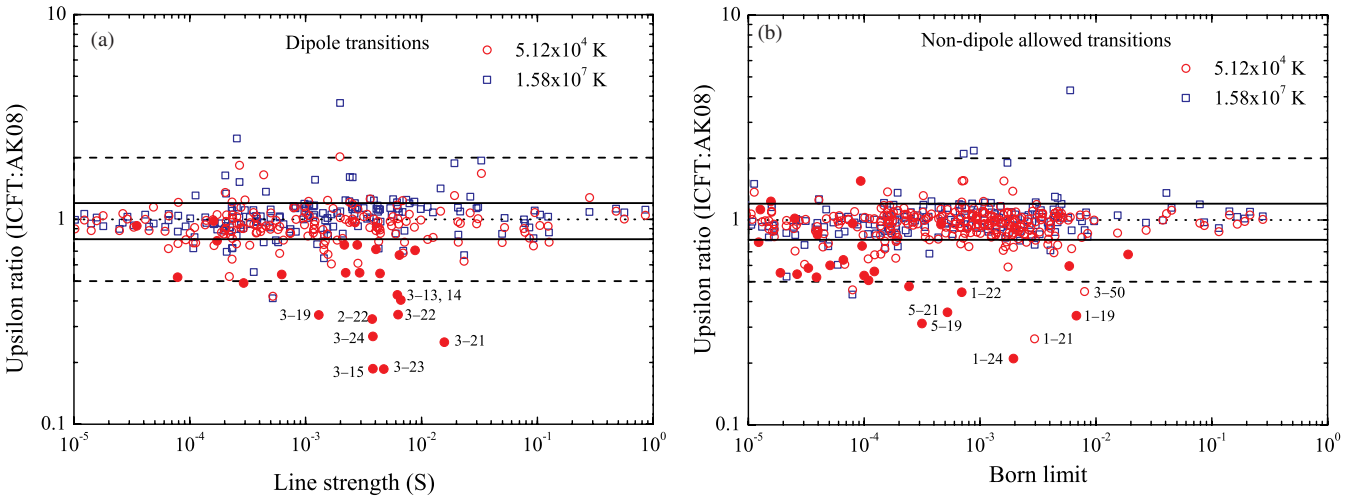

Figure 4. Scatter plot of ratios of 'undamped' effective collision strengths from the present ICFT *R*-matrix calculation and the DARC calculation of Aggarwal and Keenan (2008) as a function of the present AS (a) line strength (*S*) (for dipole transitions) and (b) Born-limit (non-dipole allowed transitions). '○' and '●' symbols denote transitions at 5.12×10^4 K with threshold energy differences between ICFT and AK08 calculations being less than and greater than 0.2 Ryd, respectively. '□' symbols: corresponding results at 1.58×10^7 K. Solid and dashed lines correspond to agreement within 20% and a factor of 2, respectively. Dotted lines mark where the ratios agree.

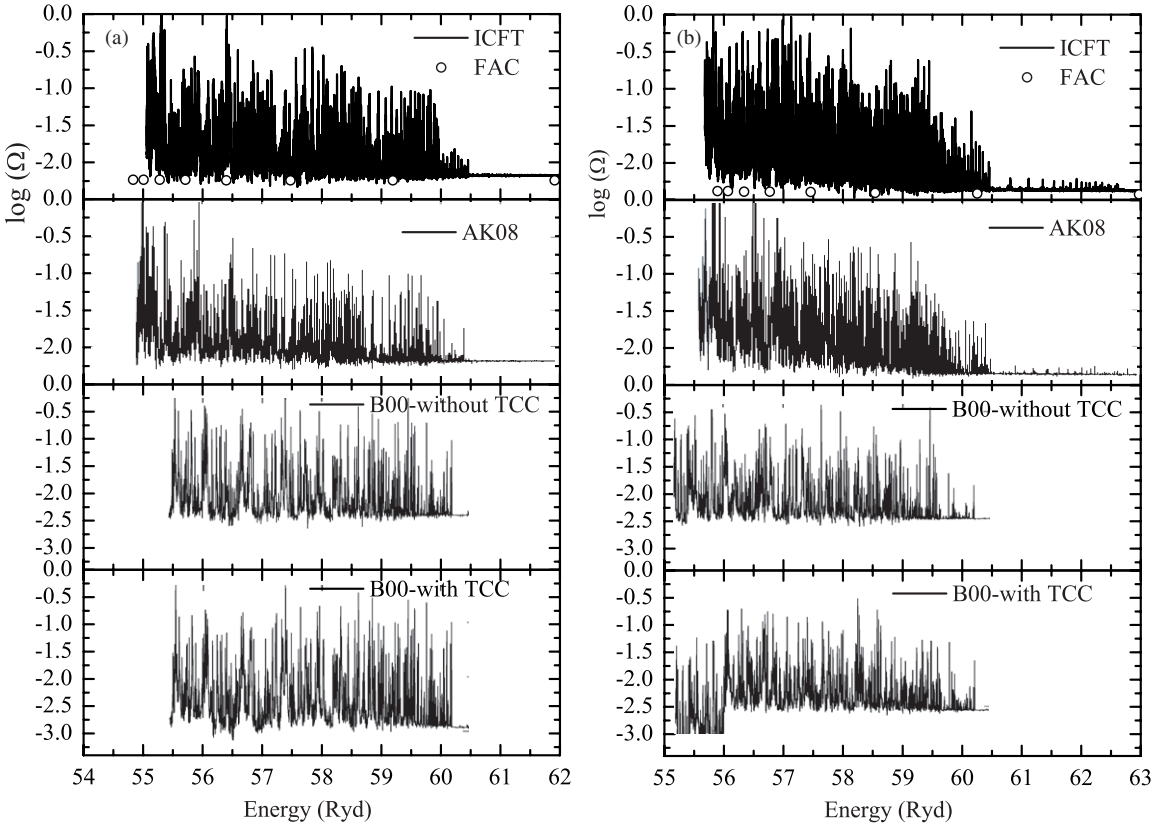

Figure 5. Collision strengths (Ω) from the ICFT *R*-matrix (present work), DARC (AK08) and JAJOM (Bautista (2000): B00) calculations. (a) For 1–15 ($2s^2 2p^6 3s\ ^2S_{1/2}$–$2s^2 2p^5 3s3p\ ^2S_{1/2}$) transition line. (b) 1–21 ($2s^2 2p^6 3s\ ^2S_{1/2}$–$2s^2 2p^5 3s3p\ ^2D_{5/2}$) transition line. '○' denote DW values obtained from FAC (present work).

up to $J = 12$ were included in the exchange calculation. The contributions from higher partial waves up to $J = 42$ were included via a non-exchange calculation. A 'top-up' was used to complete the partial collision strength sum over higher J-values by using the Burgess sum rule (Burgess 1974) for dipole transitions and a geometric series for the non-dipole transitions (Badnell and Griffin 2001). In the outer-region calculation, we used an energy mesh step of $2 \times 10^{-6} z^2$ Ryd through the resonance region (from threshold to 72 Ryd), where z is the residual charge of the ion (15 in the present case). Beyond the resonance region (from 72 to 450 Ryd), for the exchange calculation, an energy step of $2 \times 10^{-4} z^2$ Ryd was used. For

the non-exchange calculation, we used a step of $1 \times 10^{-3} z^2$ Ryd over the entire energy range. The calculation was carried-out up to an incident energy of 450 Ryd. We used the infinite energy Born limits (non-dipole allowed) and line-strengths (dipole-allowed) from AUTOSTRUCTURE so that the collision strengths could be interpolated at any desired energy when Maxwell-averaging (see Whiteford *et al* (2001)).

Observed energies were used for the lowest 25-lying levels. For those levels missing from the NIST database, we first derived the mean value of differences between our level energies and the corresponding NIST values for available levels of the $2s^2 2p^5 3s3p$ configuration, then we adjusted our calculated level energies by this mean value. These observed and adjusted energies are employed in the MQDT formula which converts from the slowly-varying-with-energy unphysical K-matrix to the strongly (resonant) energy-dependent physical K-matrix. This ensures that Rydberg series of resonances converge on the observed thresholds. In addition, low-lying (non-correlation) resonances can be expected to be positioned accurately just above excitation thresholds. A similar procedure has been demonstrated to be very accurate in the study of dielectronic recombination, where there is much precise experimental cross-section data with which to compare with (see Savin *et al* (2002), for example).

In figure 3, we show the collision strength of the $2s^2 2p^6 3s\ ^2S_{1/2}$–$2s^2 2p^5 3s^2\ ^2P_{3/2}$ transition line, both without damping[4] as well as with Auger-plus-radiation damping. The reduction due to the effect of Auger-plus-radiation damping is very apparent on resonances, especially at higher energies, and can be up to two orders of magnitude. Some resonances are completely damped. The damping is dominated by far (∼90%) by the Auger process for $n > 3$. We also performed a distorted-wave (DW) calculation by using the FAC code with the same configuration interactions as in our 134-level ICFT R-matrix calculation. For this 1–6 transition, the DW data is lower than the background value obtained from R-matrix by 25% at 8 Ryd.

Generally speaking, Maxwell-averaged effective collision strengths (Υ) have a more extensive application than the ordinary collision strengths (Ω), in addition to the advantage of a much smaller storage size. Test calculations show that the effective collision strengths have converged (to within 1% for 87% of transitions) down to a temperature of 5.12×10^4 K on using an energy mesh step of $2 \times 10^{-6} z^2$ Ryd. At high temperatures, effective collision strengths have converged on using a much coarser mesh step of $5 \times 10^{-6} z^2$ Ryd. So, in our following work, we adopt an energy step of $2 \times 10^{-6} z^2$ Ryd, which is smaller than that adopted by AK08, by a factor of 2.

4. Results and discussions

4.1. Comparison of undamped results: the ICFT R-matrix versus DARC

We make comparison with the results of AK08 calculated by using DARC. We make contrasting comparisons at a low temperature (5.12×10^4 K) and a high one (1.58×10^7 K) as shown in figure 4, in which transitions from the lowest 5-lying levels to all higher levels (total 655 transitions) are plotted for dipole allowed (211) and non-dipole allowed (426) transitions. In intermediate coupling, spin–orbit mixing means that very few transitions that were forbidden in LS-coupling remain so. Instead, they have small but non-zero line strengths or infinite energy Born limits. Indeed, only 18 transitions from the lowest 5-lying levels are strictly forbidden according to this definition (and are not shown in figure 4).

[4] Of course, $n = 3$ Auger damping is still present here as it is intrinsic to the close-coupling expansion.

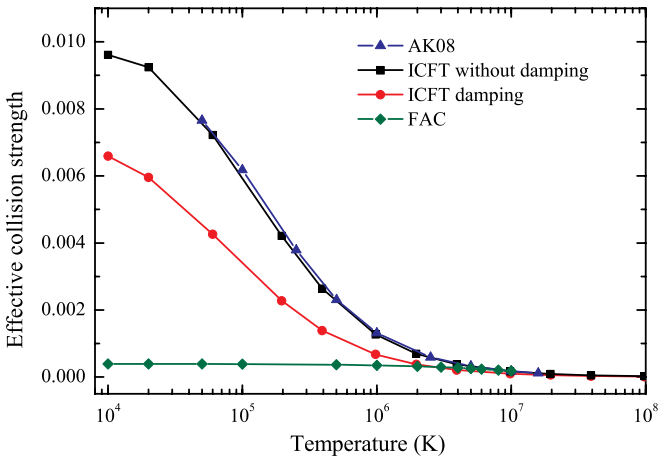

Figure 6. Comparison of the effective collision strengths for the $2s^2 2p^6 3s\ ^2S_{1/2}$–$2s^2 2p^5 3p^2\ ^4P_{5/2}$ transition (1–28). The ICFT R-matrix and FAC DW are present results. AK08 denotes the DARC results of Aggarwal and Keenan (2008).

Table 3. Excitation energies (Ryd) used for dipole transitions with large differences at low temperatures between the ICFT and DARC effective collision strengths.

i	j	ICFT[a]	DARC[b]	ICFT–DARC
1	6	52.60745	52.31155	0.29589
1	7	53.51871	53.22823	0.29048
2	8	51.74576	51.51313	0.23263
2	11	52.05286	51.83545	0.21741
2	12	52.15916	51.95366	0.20550
2	15	52.53278	52.28154	0.25124
2	17	52.96107	52.73537	0.22570
2	22	53.32558	53.01148	0.31410
2	23	53.92686	53.69872	0.22814
2	24	54.12749	53.85740	0.27009
3	8	51.55486	51.33900	0.21586
3	9	51.79511	51.57144	0.22367
3	11	51.86196	51.62987	0.23209
3	13	52.08980	51.86496	0.22485
3	14	52.07754	51.86496	0.21259
3	15	52.34188	52.10219	0.23969
3	17	52.77017	52.55290	0.21727
3	19	52.91628	52.67441	0.24187
3	22	53.13468	52.82709	0.30759
3	23	53.73596	53.50953	0.22643
3	24	53.93659	53.66709	0.26949
4	6	46.45183	46.11676	0.33507
4	7	47.36309	47.04529	0.31780
5	6	46.42536	46.09344	0.33192

[a] Present work.
[b] Aggarwal and Keenan (2008).

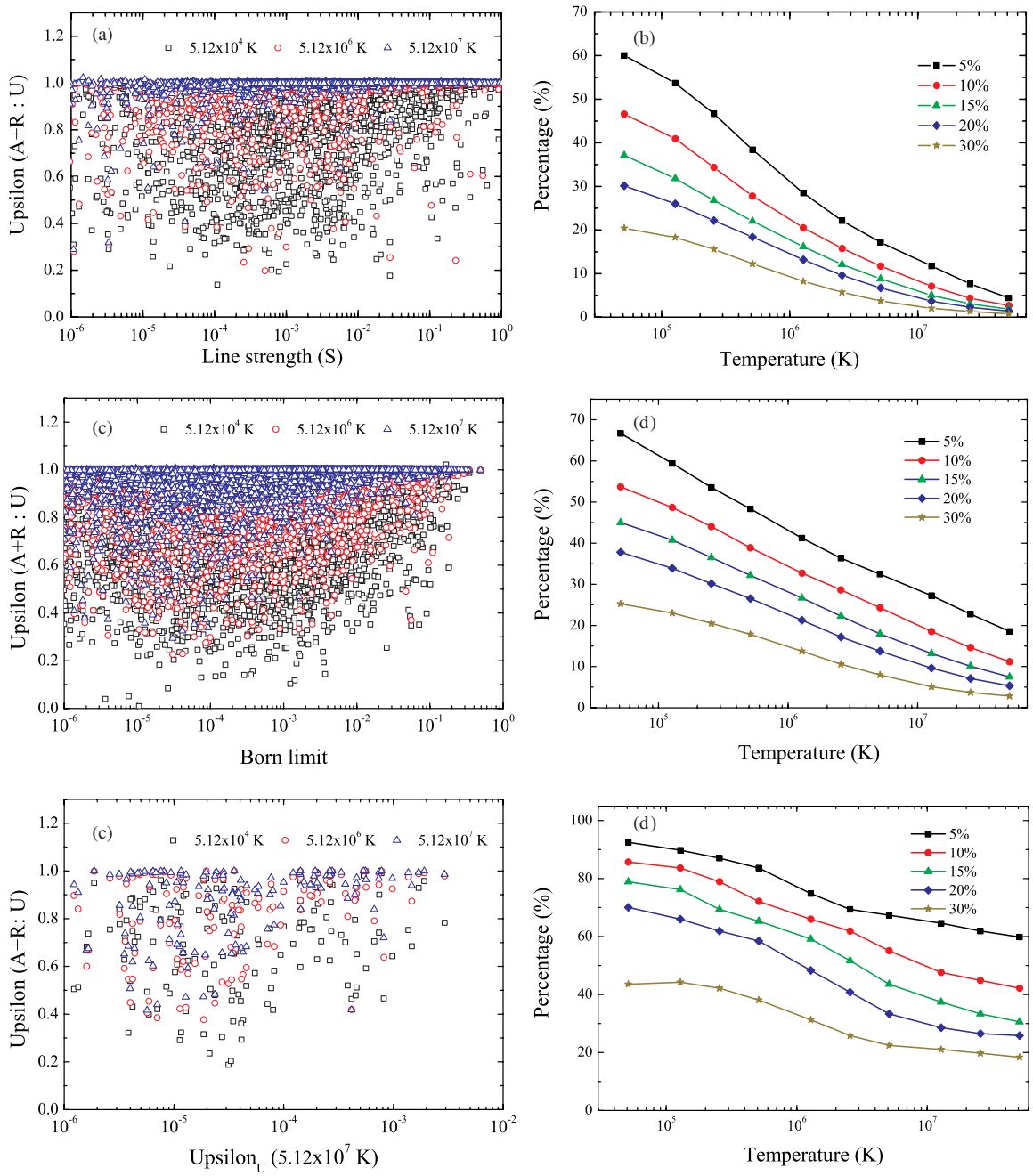

Figure 7. Left-hand panels: scatter plots showing the ratio of the effective collision strengths (Υ) with Auger-plus-radiation damping (Upsilon(A+R)) to without damping (Upsilon_U) as a function of (a) line strength, (c) infinite temperature Born limit, (e) undamped Υ at the highest tabulated temperature (5.12×10^7 K), for dipole, non-dipole allowed and forbidden transitions, respectively. Right-hand panels: percentage of corresponding transitions where the effect of damping exceeds 5%, 10%, 15%, 20% and 30%.

For most transitions, our undamped ICFT *R*-matrix results agree with the DARC ones of AK08, to within 20% over the entire temperature range. At the low temperature (5.12×10^4 K), there are 35.5% of dipole and 20.7% of non-dipole allowed transitions with a difference of over 20%. This difference decreases to 25.1% of dipole and 13.8% of non-dipole allowed transitions at the high temperature (1.58×10^7 K) and at the low temperature (5.12×10^4 K). Here, for dipole transitions, we find that there is a strong correlation between the ratio of the ICFT to DARC Υ values and the ratio of the AS to GRASP line strengths. The ICFT/DARC agreement for non-dipole allowed transitions should also be strongly correlated with the atomic structure—this time for the infinite energy Born limit, but we do not have such results for GRASP.

In figure 4, we identify a group of dipole and non-dipole allowed transitions (see table 3) for which the ratio of line strengths (electric dipole only) is close to unity but the DARC effective collision strengths are systematically larger than those obtained from ICFT, at the lower temperature. This is probably due to the smaller excitation energies used by AK08 (recall, we adjusted to observed) which means that there are additional resonances present at lower energies/temperatures

Table 4. Undamped (U) and Auger-plus-radiation damped (A+R) effective collision strengths $\Upsilon_{i,j}$, at the given temperatures.

		5.12×10^4 K		5.12×10^5 K		5.12×10^6 K	
i	j	U	A+R	U	A+R	U	A+R
1	2	1.38(+0)[a]	1.37(+0)	1.22(+0)	1.22(+0)	1.51(+0)	1.51(+0)
1	3	2.28(+0)	2.30(+0)	2.40(+0)	2.40(+0)	2.99(+0)	2.99(+0)
1	4	1.27(−1)	1.27(−1)	1.28(−1)	1.28(−1)	1.46(−1)	1.43(−1)
1	5	1.90(−1)	1.90(−1)	1.92(−1)	1.92(−1)	2.19(−1)	2.14(−1)
1	6	1.56(−1)	5.25(−2)	8.28(−2)	3.08(−2)	1.64(−2)	9.04(−3)
1	7	8.20(−2)	3.67(−2)	4.12(−2)	1.79(−2)	8.38(−3)	4.87(−3)
1	8	5.58(−2)	3.08(−2)	2.17(−2)	1.43(−2)	6.27(−3)	5.29(−3)
1	9	5.32(−2)	2.88(−2)	2.06(−2)	1.21(−2)	5.56(−3)	4.39(−3)
1	10	5.39(−2)	3.69(−2)	2.12(−2)	1.54(−2)	6.28(−3)	5.48(−3)
1	11	3.14(−2)	1.67(−2)	1.34(−2)	7.34(−3)	4.12(−3)	3.26(−3)
1	12	1.74(−2)	7.07(−3)	7.60(−3)	3.75(−3)	2.13(−3)	1.60(−3)
1	13	3.84(−2)	1.47(−2)	1.45(−2)	7.08(−3)	4.02(−3)	3.03(−3)
1	14	4.00(−2)	1.85(−2)	1.67(−2)	9.85(−3)	4.99(−3)	4.08(−3)
1	15	4.19(−2)	2.27(−2)	1.75(−2)	1.12(−2)	7.94(−3)	7.04(−3)
1	16	1.38(−2)	7.14(−3)	6.78(−3)	3.60(−3)	1.73(−3)	1.25(−3)
1	17	2.66(−2)	1.39(−2)	1.32(−2)	6.97(−3)	3.73(−3)	2.82(−3)
1	18	1.51(−2)	6.32(−3)	7.76(−3)	3.53(−3)	2.21(−3)	1.60(−3)
1	20	2.67(−2)	1.39(−2)	1.46(−2)	7.66(−3)	3.66(−3)	2.61(−3)
1	19	3.71(−2)	2.09(−2)	1.70(−2)	1.02(−2)	5.99(−3)	5.00(−3)
1	21	4.38(−2)	2.24(−2)	1.94(−2)	9.99(−3)	5.69(−3)	4.34(−3)
1	22	3.45(−2)	1.46(−2)	1.59(−2)	7.09(−3)	3.53(−3)	2.26(−3)
1	23	3.86(−2)	2.63(−2)	3.22(−2)	2.30(−2)	1.90(−2)	1.75(−2)
1	24	2.42(−2)	1.10(−2)	1.02(−2)	5.86(−3)	3.22(−3)	2.62(−3)
1	38	7.23(−3)	3.76(−3)	2.95(−3)	1.83(−3)	1.41(−3)	1.27(−3)
1	39	4.26(−3)	2.46(−3)	2.36(−3)	1.76(−3)	1.73(−3)	1.65(−3)
1	25	9.07(−2)	8.37(−2)	8.61(−2)	8.08(−2)	8.35(−2)	8.26(−2)
1	43	7.58(−3)	4.53(−3)	2.15(−3)	1.13(−3)	2.98(−4)	1.71(−4)
1	42	6.52(−3)	3.70(−3)	3.23(−3)	2.05(−3)	1.23(−3)	1.08(−3)
1	44	7.51(−3)	3.65(−3)	3.01(−3)	1.79(−3)	1.44(−3)	1.30(−3)
1	46	6.50(−3)	3.02(−3)	2.49(−3)	1.31(−3)	6.90(−4)	5.45(−4)
1	48	5.04(−3)	1.88(−3)	1.35(−3)	4.82(−4)	1.84(−4)	7.99(−5)
1	53	3.10(−3)	1.27(−3)	1.13(−3)	6.25(−4)	5.14(−4)	4.53(−4)
1	49	5.05(−3)	2.67(−3)	1.65(−3)	8.32(−4)	3.54(−4)	2.52(−4)
1	52	5.34(−3)	2.47(−3)	1.70(−3)	7.64(−4)	3.08(−4)	1.93(−4)
1	54	3.65(−3)	1.47(−3)	1.21(−3)	6.31(−4)	4.50(−4)	3.82(−4)
1	58	5.18(−3)	2.01(−3)	1.81(−3)	9.03(−4)	5.36(−4)	4.29(−4)
1	55	6.96(−3)	5.05(−3)	4.61(−3)	4.11(−3)	2.80(−3)	2.74(−3)
1	59	1.17(−2)	9.16(−3)	8.58(−3)	7.80(−3)	5.53(−3)	5.44(−3)
1	56	5.52(−3)	2.43(−3)	2.39(−3)	1.38(−3)	8.74(−4)	7.50(−4)
1	57	4.91(−3)	1.66(−3)	1.94(−3)	8.33(−4)	5.58(−4)	4.21(−4)
1	60	1.27(−2)	9.56(−3)	9.18(−3)	8.14(−3)	5.29(−3)	5.16(−3)
1	63	1.31(−2)	1.04(−2)	9.78(−3)	8.92(−3)	5.89(−3)	5.79(−3)
1	61	1.01(−2)	7.06(−3)	6.92(−3)	6.00(−3)	4.13(−3)	4.02(−3)
1	66	1.65(−3)	5.00(−4)	5.56(−4)	1.51(−4)	7.43(−5)	2.45(−5)
1	70	9.28(−3)	5.77(−3)	5.58(−3)	4.62(−3)	3.36(−3)	3.25(−3)
1	67	5.48(−3)	1.67(−3)	1.82(−3)	8.44(−4)	5.88(−4)	4.73(−4)
1	74	5.77(−3)	3.10(−3)	3.20(−3)	2.45(−3)	1.71(−3)	1.62(−3)

[a] (m) denotes $\times 10^m$.

in the AK08 data. This can be tested indirectly by looking at excitations to higher levels, which also have strong resonant contributions. For example, for the 1–28 transition (not shown) with a threshold energy difference of 0.041 Ryd, the Υ values are 7.58×10^{-3} and 7.61×10^{-3}, respectively, at the low temperature.

AK08 selected the 1–15 and 1–21 transitions to reveal inadequacies of term-coupling via the JAJOM code, as used by Bautista (2000), which results in the sudden increase and/or decrease of background collision strengths when relativistic effects are included for some transitions (see figure 3 in Bautista (2000) and the bottom two panels in figure 5). This is exactly the same inadequacy demonstrated originally by Griffin *et al* (1998) when they introduced the ICFT *R*-matrix method to solve the problem, without resorting to a full Breit–Pauli (or Dirac) calculation. AK08 conclude that this inadequacy is the reason for the large discrepancies between the results of their two calculations. In order to illustrate the inadequacy of the JAJOM method and the overestimation of AK08 at the lower temperature for some transitions (see filled circles in figure 4(a)), we compare the underlying collision strengths for 1–15 and 1–21 transitions in figure 5. We see that the background does not shift down and no sudden jumps appear in the present ICFT results, in contrast to that seen from

JAJOM—see the bottom two panels of figure 5. The background of ICFT Ω-values show excellent agreement with the DARC ones. Our DW results obtained from FAC are also overlapped, showing an excellent agreement with the background result of the two *R*-matrix calculations. Additionally, the resonance structures in the two *R*-matrix calculations basically agree with each other. However, because the energy of $2s^22p^53s3p\ ^2S_{1/2}$ (15-) and $^2D_{5/2}$ (21-) levels of the AK08's data are lower than the observed values which we use, by ≈0.2 Ryd, resonances around this region appear in the work of AK08, as shown in figure 5. So, their results are probably somewhat of an overestimate of the effective collision strengths at lower temperatures.

4.2. Comparison of the ICFT R-matrix results: damped versus undamped

Figure 6 shows the results of several calculations of the effective collision strength (ϒ) for the $2s^22p^63s\ ^2S_{1/2}$–$2s^22p^53p^2\ ^4P_{5/2}$ transition (1–28). They demonstrate the physics we seek to describe: firstly, on comparing *R*-matrix results with our DW ones obtained with FAC, we see that the resonant enhancement is about a factor of 8 at 2×10^4 K (typical of where Fe^{15+} is abundant in photoionized plasmas); secondly, there is a close agreement between our present undamped ICFT *R*-matrix results and the DARC *R*-matrix ones of AK08; finally, Auger-plus-radiation damping lowers the resonance enhanced results by nearly a factor of 2, again at 2×10^4 K.

The widespread effect of Auger-plus-radiation damping is illustrated via a scatter plot of the ratios of damped to undamped ϒ values for dipole (figure 7(a)), non-dipole allowed (figure 7(c)) and forbidden (figure 7(e)) transitions. We see that the reduction at the low temperature (5.12×10^4 K) can be up to a factor of 3 for a few (1.3%) dipole transitions. The effect reduces with increasing of temperature and is less than 10% for 97.5% of these transitions at the high temperature (5.12×10^7 K). An illustrative way to quantify the information in the scatter plot is to count how many transitions differ by more than a given amount. In figure 7(b), we show the percentage of each class of transition where the damping effect is at least 5%, 10%, 15%, 20% and 30%. About 20% of dipole transitions show a damping effect of more than 30% at 5.12×10^4 K. At higher temperatures, the damping becomes a smaller effect—less than 6% of dipole transitions show a >30% effect at 2.56×10^6 K, for example. For non-dipole allowed transitions (see figure 7(c)), the damping effect can be up to a factor 3 for some transitions (2.1%) with a Born limit between 10^{-4} and 10^{-2} at the low temperature (5.12×10^4 K). The effect reduces to less than 10% for 88.7% of these transitions at the high temperature (5.12×10^7 K). Counting statistics (see figure 7(d)) reveals that ≈25% of non-dipole allowed transitions show a reduction of more than 30% at the low temperature. There are only a few forbidden transitions (1.6% of the 8911 transitions in total). The damping effect is stronger for weaker excitations, see figure 7(e). About 44% of forbidden transitions show a damping effect over 30% at the low temperature (5.12×10^4 K)—see figure 7(f). At the high temperature, the percentage is still 40% of forbidden transitions with damping over 10%. This value is significantly higher than that for dipole (2.5%) and non-dipole allowed (11.3%) transitions. We also note that the forbidden transitions are affected over a wider range of electron temperatures.

Finally, in table 4, the undamped and damped effective collision strengths are given for excitations from the ground level at three temperatures of 5.12×10^4, 5.12×10^5 and 5.12×10^6 K. The full set of data (energy levels, radiative rates and effective collision strengths) are made available through different archives and databases (the Oak Ridge Controlled Fusion Atomic Data Center (CFADC)[5] in the ADAS *adf04* format (Summers 2004), ADAS[6] and CHIANTI[7]).

5. Conclusions

The level-resolved inner-shell electron-impact excitation of Fe^{15+} has been studied via the intermediate coupling frame transformation *R*-matrix method which can allow for the inclusion of Auger-plus-radiation damping of such resonantly-excited states. The 134 levels belonging to the configurations $2s^22p^63l$, $2s^22p^53s3l$ (l = s, p and d), $2s^22p^53p^2$ and $2s^22p^53p3d$ were included in both the target configuration and close-coupling expansions. A comparison of energy levels and radiative rates with those of AK07 reveals the target structures to be comparable, and so form the basis for comparison with the excitation data of AK08.

The results of our undamped ICFT *R*-matrix calculation agree well with the undamped DARC effective collision strengths of AK08 for most excitations. For a few transitions, their results are higher than ours by a factor of two at low temperatures. This is probably due to their use of smaller theoretical transition energies than ours, which were adjusted to the observed values. When Auger-plus-radiation damping is included, our results are systematically smaller than those of AK08. Moreover, the reduction can be up to a factor of 3 for some transitions. The number of transitions where the reduction of ϒ exceeds 20% occupies 30.2%, 37.7% and 70.7% of dipole, non-dipole allowed and forbidden transitions, respectively, at the low temperatures typical of where Fe^{15+} is abundant in photoionized plasmas.

In summary, Auger-plus-radiation damping plays an important role on the electron-impact excitation of inner-shell transitions. Thus, for many transitions, the results of previous undamped inner-shell calculations overestimate the effective collision strengths significantly.

Acknowledgments

The work of the UK APAP program is funded by the UK STFC under grant no. PP/E001254/1 with the University of Strathclyde. One of us (GYL) would like to thank M C Witthoeft for some helpful discussions.

[5] http://www-cfadc.phy.ornl.gov/data_and_codes
[6] http://www.adas.ac.uk/
[7] http://www.chianti.rl.ac.uk/

References

Aggarwal K M and Keenan F P 2007 *Astron. Astrophys.* **463** 399

Aggarwal K M and Keenan F P 2008 *J. Phys. B: At. Mol. Opt. Phys.* **41** 015701

Badnell N R 1986 *J. Phys. B: At. Mol. Phys.* **19** 3827

Badnell N R and Griffin D C 1999 *J. Phys. B: At. Mol. Opt. Phys.* **32** 2267

Badnell N R and Griffin D C 2001 *J. Phys. B: At. Mol. Opt. Phys.* **34** 681

Bautista M A 2000 *J. Phys. B: At. Mol. Opt. Phys.* **33** 71

Bautista M A, Mendoza C, Kallman T R and Palmeri P 2004 *Astron. Astrophys. Suppl.* **418** 1171

Berrington K A, Ballance C P, Griffin D C and Badnell N R 2005 *J. Phys. B: At. Mol. Opt. Phys.* **38** 1667

Berrington K A, Eissner W and Norrington P N 1995 *Comput. Phys. Commun.* **92** 290

Bryans P, Badnell N R, Gorczyca T W, Laming J M, Mitthumsiri W and Savin D W 2006 *Astrophys. J. Suppl.* **167** 343

Burgess A 1974 *J. Phys. B: At. Mol. Phys.* **7** L364

Cornille M, Dubau J, Faucher P, Bely-Dubau F and Blancard C 1994 *Astron. Astrophys. Suppl.* **105** 77

Dere K P, Landi E, Young P R and Del Zanna G 2001 *Astrophys. J. Suppl.* **134** 331

Eissner W, Jones M and Nussbaumer H 1974 *Comput. Phys. Commun.* **4** 270

Gorczyca T W and Badnell N R 1996 *J. Phys. B: At. Mol. Opt. Phys.* **29** L283

Gorczyca T W and Robicheaux F 1999 *Phys. Rev.* A **60** 1216

Gorczyca T W, Robicheaux F, Pindzola M S and Badnell N R 1995 *Phys. Rev.* A **52** 3852

Griffin D C, Badnell N R and Pindzola M S 1998 *J. Phys. B: At. Mol. Opt. Phys.* **31** 3713

Gu M F 2003 *Astrophys. J.* **582** 1241

Kallman T and Bautista M 2001 *Astrophys. J. Suppl.* **133** 221

Norrington P H and Grant I P 1987 *J. Phys. B: At. Mol. Phys.* **20** 4869

Phillips K J H, Greer C J, Bhatia A K, Coffey I H, Barnsley R and Keenan F P 1997 *Astron. Astrophys.* **324** 381

Robicheaux F, Gorczyca T W, Pindzola M S and Badnell N R 1995 *Phys. Rev.* A **52** 1319

Savin D W *et al* 2002 *Astrophys. J. Suppl.* **138** 337

Summers H P 2004 The ADAS User Manual version 2.6 (http://adas.phys.strath.ac.uk)

Whiteford A D, Badnell N R, Ballance C P, O'Mullane M G, Summers H P and Thomas A L 2001 *J. Phys. B: At. Mol. Opt. Phys.* **34** 3179

Whiteford A D, Badnell N R, Ballance C P, Loch S D, O'Mullane M G and Summers H P 2002 *J. Phys. B: At. Mol. Opt. Phys.* **35** 3729

Witthoeft M C and Badnell N R 2008 *Astron. Astrophys.* **481** 543

Witthoeft M C, Whiteford A D and Badnell N R 2007 *J. Phys. B: At. Mol. Opt. Phys.* **40** 2969